

How Hydrogen Affects the Formation and Evolution of Persistent Slip Bands in High-Purity α -Iron

Florian Schaefer,* Sebastian Geyer, and Christian Motz

The effect of hydrogen on the fatigue behavior of materials has been studied extensively during the past 100 years, but is just poorly understood due to the complex interplay between hydrogen and deformation processes. In this context, hydrogen damage of metals is becoming one of the major challenges of decarbonization. While most work focuses on f.c.c. materials, the availability of relevant results becomes sparse when considering technologically highly relevant b.c.c. metals such as structural steels. This work uses in situ electrochemical hydrogen charging of α -iron steels to investigate the formation and evolution of intrusions and extrusions prior to fatigue crack initiation using a new charging setup by which the specimens are charged from the interior. The advantage of this innovative technique is that the surface of the specimens can subsequently be characterized using atomic force microscopy without artefacts from electrochemical charging or corrosion. Hydrogen is shown to enhance slip localization at the early stages of damage. The developed persistent slip lines are less pronounced. By means of transmission Kikuchi diffraction, it is shown that orientation gradients between cells in the dislocation structure are much weaker in the presence of hydrogen. Hence, hydrogen appears to promote slip reversibility in b.c.c. materials.

models such as the hydrogen-enhanced localized plasticity (HELP) mechanism have been postulated.^[6]

The HELP mechanism, which describes an enhanced slip localization and planarity in hydrogen-charged materials, has been experimentally confirmed in many studies in numerous materials.^[7–9] However, the basis of the HELP mechanism on the atomistic scale is not yet explained sufficiently. There is still a discussion of explanations. There are two main approaches. The first one postulates that a Cottrell-like hydrogen atmosphere shields the stress field of dislocations^[10–13] leading to reduced cross-slip. The second approach proposes a reduction of the stacking fault energy (SFE), partially from the same authors^[14] but with experimental evidence, e.g., by the acoustic emission technique.^[15] The latter SFE-based approach supposes an increase of the equilibrium spacing between partial dislocations and thus a lowered susceptibility to cross-slip.

But, there is no consensus that a reduction

of the SFE is the dominant origin of a more localized slip.


Ab initio studies revealed that hydrogen also reduces the Peierls potential.^[16] These studies could not affirm that a reduction of the SFE up to 40% alone promotes slip planarity. Rather, hydrogen was strongly attracted by the dislocation core, with the binding energy being determined by the dislocation character. Hydrogen changes the core structure and therefore in particular for f.c.c. Al the formation or elongation of screw segments by cross-slip increases the expense of energy.^[16] Hence, edge components are stabilized by hydrogen with experimental evidence.^[17] Subsequently, this results in a more planar slip. A change in the dislocation core and thus a dislocation character-specific line energy and Peierls potential was also derived for α -iron^[18,19] promoting this explanation. In addition, however, a drop in the SFE is likely to have a planarity-supporting contribution.^[20] Considering these discussions, the overall conclusion remains: hydrogen localizes dislocation slip in b.c.c. and f.c.c. metals.

The issue of dislocation interactions in the presence of hydrogen becomes even more complex when fatigue of materials is addressed. During fatigue, dislocations form complex networks in a multitude of dislocation reactions over thousands of load cycles.^[21] These networks that result from a competitive dislocation multiplication, rearrangement, and annihilation can ultimately lead to crack initiation.^[22] Cracks can initiate either by slip transfer blockade where persistent slip bands (PSBs) hit

1. Introduction

It can be considered proven that hydrogen interacts with lattice defects in metallic materials,^[1,2] thus affecting mechanisms of deformation. This leads to the widely known hydrogen embrittlement, especially when grain boundary cohesion is weakened.^[3,4] Although this has been known since 1875,^[5] the complex nature of hydrogen's interaction with dislocation dynamics is only roughly understood. A variety of phenomenological

F. Schaefer, S. Geyer, C. Motz
Materials Science and Methods
Saarland University
Campus D2 3, 66123 Saarbruecken, Germany
E-mail: f.schaefer@matsci.uni-sb.de

 The ORCID identification number(s) for the author(s) of this article can be found under <https://doi.org/10.1002/adem.202201932>.

© 2023 The Authors. Advanced Engineering Materials published by Wiley-VCH GmbH. This is an open access article under the terms of the Creative Commons Attribution-NonCommercial-NoDerivs License, which permits use and distribution in any medium, provided the original work is properly cited, the use is non-commercial and no modifications or adaptations are made.

DOI: 10.1002/adem.202201932

grain boundaries^[23,24] or at PSBs themselves depending on the grain size.^[21,25] The formation of dislocation structures during fatigue and especially the evolution of PSBs and how these lead to intrusions and extrusions as sources for cracks has been studied in detail in the past decades for f.c.c. materials.^[22,25,26] In contrast, for b.c.c. materials, the mechanisms of dislocation arrangement during fatigue and the origin of intrusions and extrusions are still under debate. The specific properties of the screw dislocations in b.c.c. materials with its threefold symmetry result in a slip-plane asymmetry, a high Peierls stress, and a thermally assisted slip by double kink formation and motion.^[19,26] It is worth noting that most b.c.c. materials exhibit a change from a *low temperature* to a *high temperature* slip regime around room temperature. Thus, at low strain rates and high temperatures, f.c.c.-like behavior can be observed with PSB formation based on ladder-like dislocation structures. During fatigue, the strain rates are usually high, however, so that a *low-temperature* behavior can be observed for pure b.c.c. materials, especially for α -iron. However, the number of studies regarding the evolution of dislocation structures under fatigue loading is very limited,^[27] and work on α -iron and low-carbon steel is rare.

During the early stages of fatigue in b.c.c. metals, dislocation cells^[27,28] and wall structures^[27,29,30] as well as dislocation-poor channels^[30–32] evolve. Only one work found ladder-like dislocation structures for low-carbon steel,^[31] and the reason for this is still under discussion.^[26] The formation of intrusions and extrusions is usually assigned to dislocation-poor channels in the dislocation cell structure.^[26,30,33]

The interplay between hydrogen and the arrangement of dislocations during fatigue is just scarcely studied. A smaller and more equiaxed dislocation cell structure was found in front of crack tips in the presence of hydrogen in low-carbon steel.^[34] Mine et al.^[35] found in coarse-grained pure iron that hydrogen increased the slip band spacing and thus slip localization in accordance with the literature discussed earlier (HELP mechanism). But, the slip band height is decreased too. The authors assumed that hydrogen reduces the irreversible part of plastic slip without detailed evidence.

This indicates the importance of a focused view on the evolution of fatigue damage in the pre-crack initiation phase in the presence of hydrogen for the technical highly relevant b.c.c. materials. Mechanical testing in the presence of hydrogen is challenging because hydrogen tends to gas out. Hence, in situ testing is required to guarantee a stable hydrogen concentration. In recent years, new testing methods for the hydrogen distribution in materials^[2,36] and the effect of hydrogen on the mechanical performance of materials have been established, e.g., refs. [37–40]. In this work, a setup is introduced that allows in situ hydrogen charging from the interior and thus achieving high hydrogen concentrations without the direct risk of measurement artefacts on the specimen surface. Subsequently, the results of intrusions and extrusion measurements on the specimen surface by atomic force microscopy (AFM) in peak-force (PF) tapping mode and laser scanning microscopy (LSM) are presented and discussed with respect to orientation gradients determined by transmission Kikuchi diffraction (TKD) in scanning electron microscopy (SEM) on transmission electron microscopy (TEM) lamellae, prepared by focused ion beam (FIB) with a standard lift-out technique.

2. Experimental Section

High-purity α -iron was purchased from Puronmetals, Hockenheim, Germany, an affiliated company of Allied Metals Corporation. The material-type Alliediron contains a maximum of 0.005 wt% C, 0.05 wt% Mn, 0.008 wt% P, and 0.006 wt% S. The yield strength is 200 MPa, the tensile strength 320 MPa, according to the manufacturer. The grain size is about 50 μm in the as-delivered state.

In a first step, round tensile specimens with M16 standard thread were lathed. By means of electrical discharge machining (EDM), the round tensile specimens were then eroded into flat tensile specimens and a central cavity of length 12 mm and width 1.5 mm was machined for the electrolyte by EDM, too. The residual thickness of the material membrane between the cavity and the specimen surface was 1 mm on both sides (see **Figure 1**). To exclude dislocation pinning beyond the upper yield strength

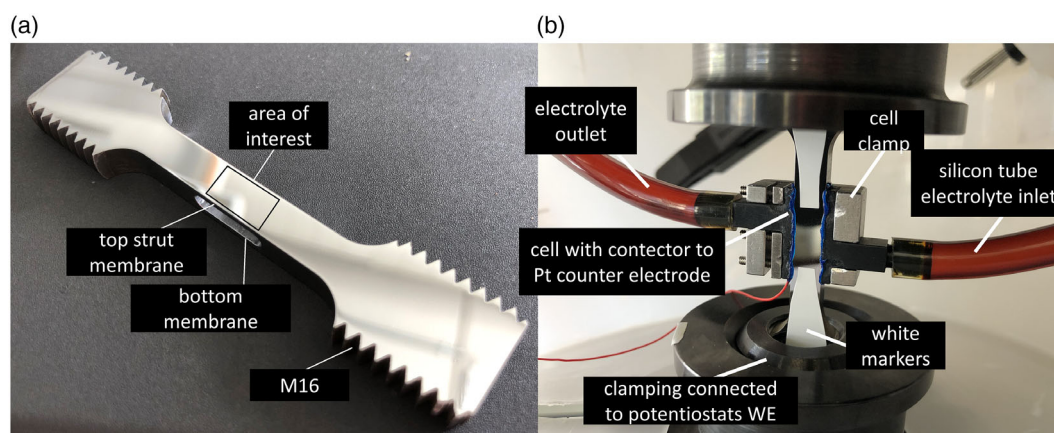


Figure 1. a) Specimen with cavity between both membrane-like strut branches; b) specimen attached to testing machine with silicon tubes conducting the electrolyte from a membrane pump through the specimen, the electrochemical cell itself and white markers attached to the upper and lower part of the specimen surface for the video extensometer. The cell consists of an in- and outlet as well as a nonvisible Pt foil as counter electrode. The cell is glued to the specimen with blue sealing agent and is clamped additionally to the specimen with a metallic clamping device.

by a Cottrell effect, the specimens were pre-stretched to a maximum of 1% elongation up to 220 MPa at maximum.

The specimens were ground and polished in multiple stages with oxide final polishing suspension OP-A from Struers, Willich, Germany. Each polishing level was done for at least 10 min to guarantee a excellent surface quality with very low roughness.

The electrochemical cell was built around the specimens and their cavity. Two polyvinyl chloride (PVC) adaptors connect the tubes for electrolyte supply and outlet to the hole, sealed with a sealing agent. Special attention was payed to removing bubbles during charging by adjusting the setup. Electrolyte was pumped through the specimens with an external membrane pump. A small Pt foil embedded in the left-hand PVC adaptor served as an inert counter electrode (CE), which was contacted from the outside by a wire cable (red wire cable in Figure 1). The electrical circuit was closed by contacting the specimen itself via the mounts as the working electrode (WE). The cell was additionally clamped to the specimens by metallic clamping devices to avoid leakage and to stabilize the system especially during attachment and removal of the specimens for the AFM and LSM measurements. The specimen membrane branches thus were charged with H (or not for the uncharged reference specimen) from the backside with a current of about 10 mAcm^{-2} . The electrolyte is 2 molar boric acid in distilled water with 5 g L^{-1} potassium iodide and 0.5 molar borax. The electrochemical potential was about 2.8 V during galvanostatic charging. Prior to the fatigue tests, the specimens were precharged for 5 d and then recharged again for one day between the AFM and LSM measurements to ensure that the hydrogen concentration in the material was at steady-state concentration and effusion artefacts could be neglected. The reference specimen was held in open-circuit potential (current of 0 A).

Next, fatigue was carried out with a resonance testing system Mikrotron from Russenberger Pruef-maschinen, Neuhausen a. R., Switzerland, with stress amplitudes between 105 and 175 MPa but in displacement control. Step-wise load increase tests were conducted with 4 displacement amplitude steps of 12, 14, 16, and $18 \mu\text{m}$ at a stress ratio of $R = -1$ and at a frequency (resonance) of approximately 152 Hz at room temperature (see Figure 2). Strain was measured during the test using a high-speed video extensometer and markers attached to the specimens. It was found that displacement and strain amplitude were largely proportional to each other (see Table 1). However, the strain measurement data suffered considerably from artefacts due to leaking electrolyte drops at the edge of the adhesive bonds to the charging cell, so that strain control was not possible here but not necessary. The tests were stopped at a significant frequency drop of about 1 Hz. Cracks in the specimens could not be tolerated, otherwise the corrosive electrolyte would have sprayed out of the specimens.

During fatigue, AFM images were acquired after 200 000 load cycles on each displacement amplitude level. A steady-state situation of the dislocation structure is expected to have evolved, then. Images are taken in PF tapping mode (Scanasyt) on a Dimension Icon from Bruker Nano Surface, Tuscon, AZ, USA, with SCANASYST-AIR tips with a declared tip radius of 2 nm. The scan field size was 60×60 – $80 \times 80 \mu\text{m}^2$. This allows at least one grain to be completely captured because the average grain

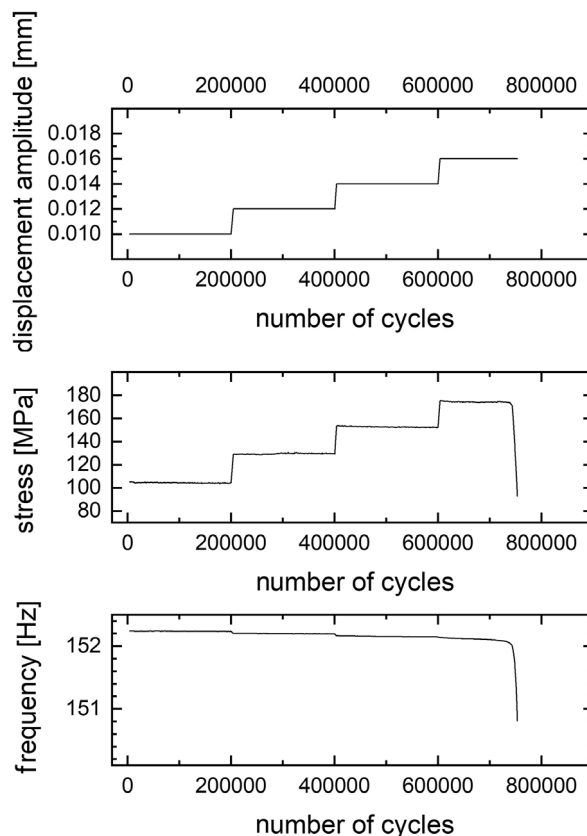


Figure 2. Evolution of applied displacement amplitude at 4 load steps and the corresponding stress amplitude and test frequency. While fracture can be easily monitored by a decrease in the stiffness of the specimens and hence in the resonance frequency, no considerable hardening or softening could be observed, as expected for b.c.c. materials. Only every 1000th load cycle can be saved at the resonance testing machine. Thus, no evolution of hardening or softening could be monitored that usually happens mostly during the first 1000 load cycles after increasing the displacement amplitude. No distinct difference could be observed between the reference and H charged specimens.

Table 1. Parameters of the load steps during the step-wise load increase test (load range from different specimens and strain amplitude are in a quasi steady-state after 1000 load cycles).

Displacement amplitude [μm]	Load amplitude [MPa]	Strain amplitude [%]
12	105–108	0.051
14	126–129	0.062
16	150–153	0.074
18	170–175	0.085

size is about $50 \mu\text{m}$. In order to obtain images of larger areas, additional images were acquired with a LSM LEXT OLS4000 from Olympus, Tokyo, Japan. Here, the scan field was $256 \times 256 \mu\text{m}$, so that this acquired about 30–40 grains at once. Three specimens were examined, two charged specimens and one reference specimen. Sufficient statistical evidence is provided by the fact that at least 10 measurements of the surface topography were carried out

in the AFM at randomly selected positions for each specimen and load step represented here. LSM measurements were performed at the third displacement amplitude level of 16 μm displacement amplitude. All specimens failed at 18 μm .

In a final step, since all specimens ruptured at a displacement amplitude level of 18 μm , two specimens, one reference, and one charged specimen were removed after the 3th load step of 16 μm displacement amplitude. TEM thin-film lamellae were prepared using a standard lift-out technique at a Helios Nanolab 600 Ga-FIB, FEI Company, Hillsboro, OR, USA. The final thinning was performed at 50 pA. Scanning transmission electron microscopy (STEM) images were taken in bright-field mode on the same microscope, and TKD measurements were performed on a Hikari system with the software TSL OIM, EDAX Ametek, Berwyn, PA, USA. Orientation gradient mapping (OGM) maps as kernel average misorientation (KAM) maps with a maximum misorientation angle of 2° were evaluated with the Channel 5 software package from Oxford Instruments, Abingdon, UK, and histograms of the misorientation angles (point-to-point, not KAM) are plotted and fitted with a Rayleigh distribution with MATLAB.

3. Results

3.1. Atomic Force Microscopy and Laser Scanning Microscopy Imaging

Selected images from AFM topography measurements and optical microscopy with Nomarski interference contrast are shown in **Figure 3**. With increasing displacement amplitude level, the number of grains with intrusions and extrusions increases. At 16 μm , displacement amplitude nearly all grains contain intrusions and extrusions.

Unexpectedly, the distribution of the intrusions and extrusions over those grains that contain them is comparable between

the individual grains. Furthermore, the heights of the extrusions are similar.

3.2. Topography Analysis

It is difficult to evaluate the data in a systematic and precise process. Either the evaluation is done by extracting individual surface profiles or by measuring typical surface parameters such as roughness or waviness. The first approach bears the risk that the evaluation is corrupted by the choice of the extracted profiles. Furthermore, this approach is very time consuming and, especially with regard to the homogeneous distribution of the intrusions and extrusions as a result of the typical noncrystallographic but wavy slip behavior in b.c.c., it is not expedient. Intrusions and extrusions lie with only a small deviation angle perpendicular to the loading axis because they follow the plane of highest shear stress.^[41] The in-depth angle remains unknown and causes a typical scattering of the data. Furthermore, due to the elaborated metallographic preparation, the surface roughness is initially below 2 nm. Thus, an automated evaluation via the surface parameters roughness average R_a and average wavelength λ_a , representing the spacing between the intrusions and extrusions, has been carried out. The results can be found in **Figure 4**. The LSM analysis allows for a more detailed view to the data. Here, the surface topographies were assessed by the extraction of individual profiles to validate the assessment by surface roughness analysis. But, this evaluation was just performed for the displacement amplitude level of 16 μm because of the very high effort of this data analysis method.

It is worth noting that with AFM, due to the finite tip radius, the height of the sharp extrusions can be more accurately determined as the depth of the intrusions, as there is no guarantee that the tip can reach the deepest point. A similar situation, although not as severe, applies to LSM measurements.

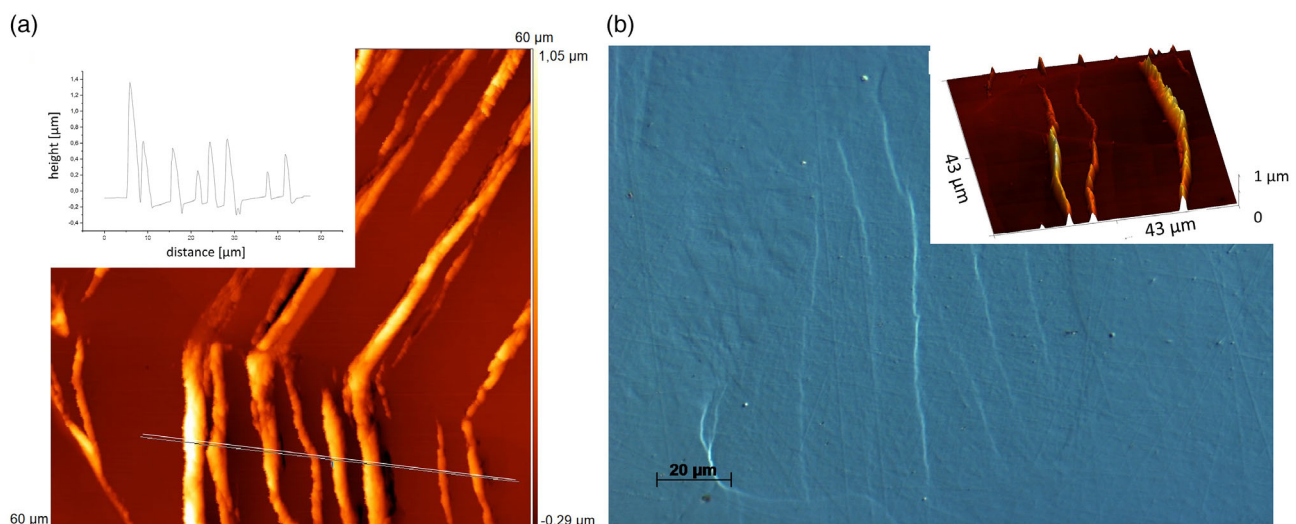


Figure 3. a) AFM topography image from uncharged specimen at 16 μm displacement amplitude. The detail shows the surface profile along the white line; b) specimen surface from optical microscope with Nomarski interference contrast at 14 μm displacement amplitude of H charged specimen, the detail shows a corresponding AFM topography scan.

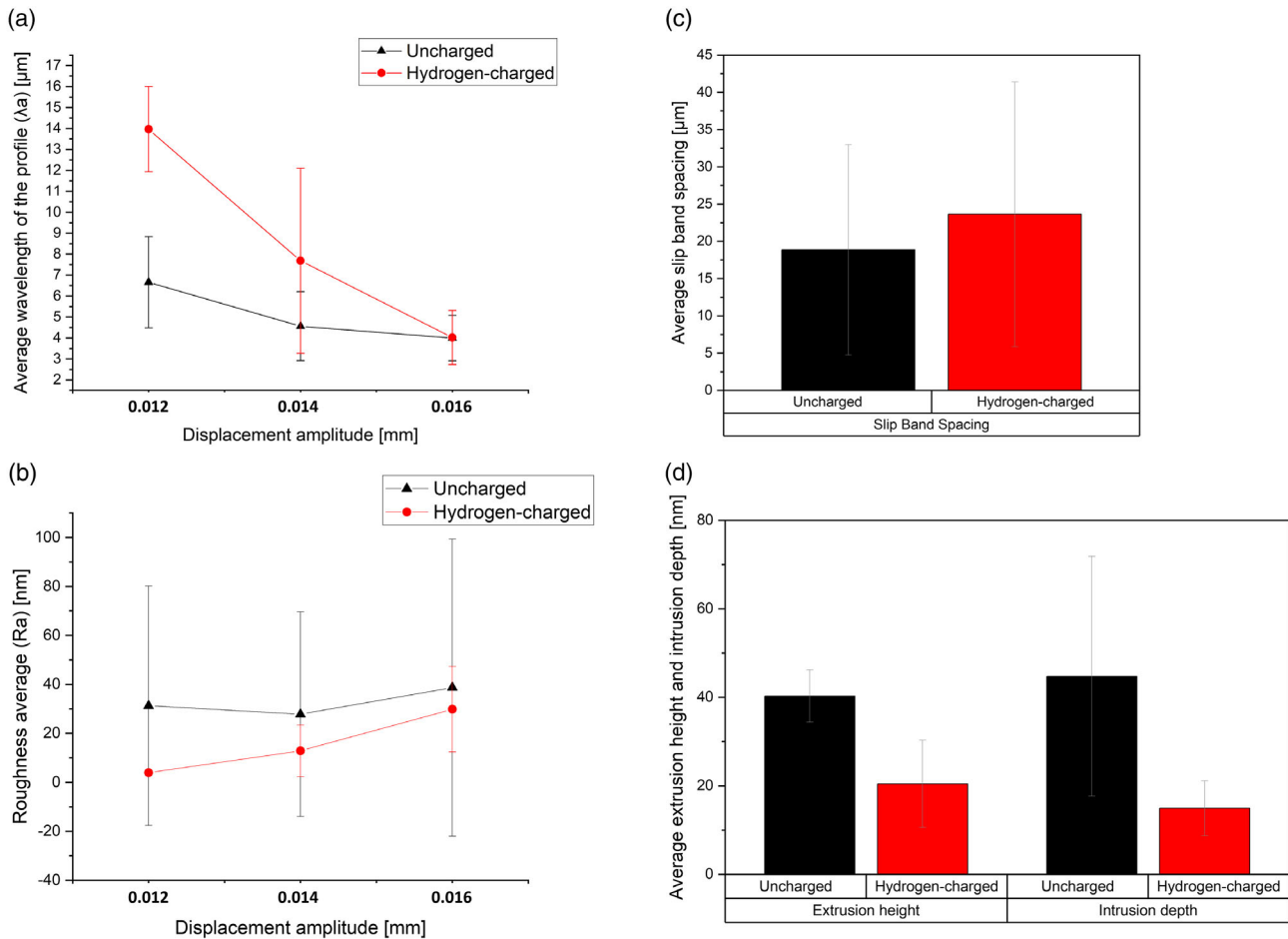


Figure 4. a,b) Evolution of the surface roughness parameters R_a and λ_a depending on the applied displacement amplitude after 200 000 load cycles on the specific displacement amplitude level, c,d) evaluation of average slip band spacing as well as extrusion height and intrusion depth from LSM measurement at 16 μm displacement amplitude after 200 000 load cycles.

3.3. STEM Imaging and Orientation Gradient Mapping

While a random orientation noise in three dimensions is best described by a Maxwell distribution of misorientations, in the case of dislocation structures, this is a Rayleigh distribution.^[42] A Rayleigh distribution describes experimental data best that result from an equivalent contribution of 2 dislocation sets with perpendicular rotational axes in a boundary. This can be regarded here as a sufficient assumption for the structure of the dislocation cells boundaries. However, it should be noted that in the case of more complex structures within the boundaries, the distribution corresponds to a superposition of two Rayleigh distributions. Since all distributions are very similar in shape but not in their parameters (mean, standard deviation) and the distributions are only fitted for visualization, and the results are not quantified further, the simple Rayleigh distribution approach was chosen here. One can clearly see in the STEM images and KAM maps in **Figure 5** that the orientation gradients at the cell boundaries without hydrogen are more pronounced, which is ultimately reflected in a broader misorientation distribution.

4. Discussion

4.1. Slip Band Spacing and Height

It is quite obvious that hydrogen localizes dislocation motion. This can be attributed to the HELP mechanism. The spacing of the slip bands (intrusions and extrusions) increases due to hydrogen charging. A similar behavior was found by Abraham et al.^[43] for austenitic steel. With increasing load amplitude, the spacing of the slip bands decreases and the proportion of those grains with slip bands increases. A similar behavior was observed by Mine et al.^[35] However, they did not increase the displacement amplitude level but the number of load cycles at constant load amplitude. During fatigue of the preloaded ferritic specimens, the distance between the slip bands decreased with increasing number of load cycles, while an offset remained between the H loaded and the H free reference specimen. In contrast, in the present study in which effusion can be excluded due to in situ charging, the slip band spacing coincides below the displacement amplitude level that ultimately leads to failure.

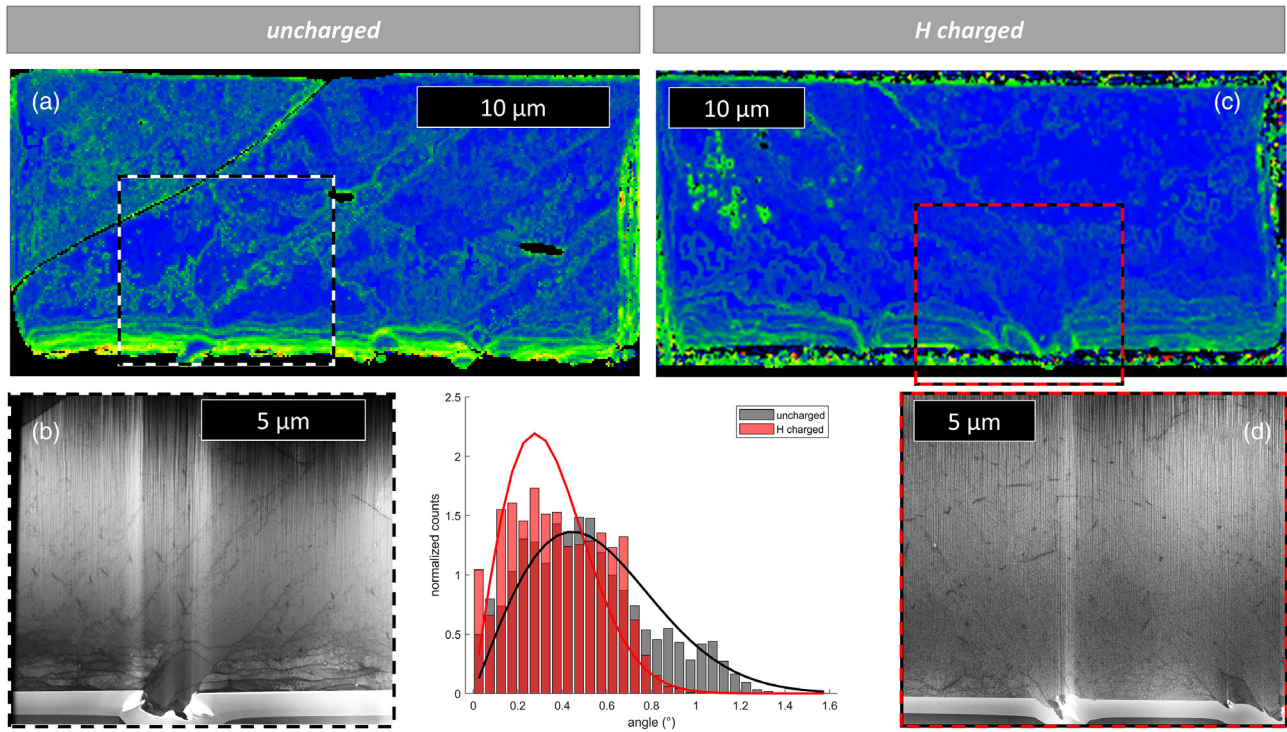


Figure 5. Top: Kernel average misorientation (KAM) maps from orientation data, acquired by transmission Kikuchi diffraction (TKD) in a scanning electron microscope (SEM) on lamellae lifted out by focused ion beam standard technique. The images on the right-hand side (c,d) represent the H charged case, whereas the images on the left-hand side (a,b) are from an uncharged specimen. The color bars of the KAM maps scale from 0 to 2°. Bottom: corresponding STEM images from the SEM in bright-field mode ((b) without H, (d) with H). e) the histograms show the misorientation distributions and the corresponding Rayleigh fits of the histogram data between 0 and 2°. It is obvious that orientation gradients between the dislocation cells are less prominent for the H charged compared to the uncharged case.

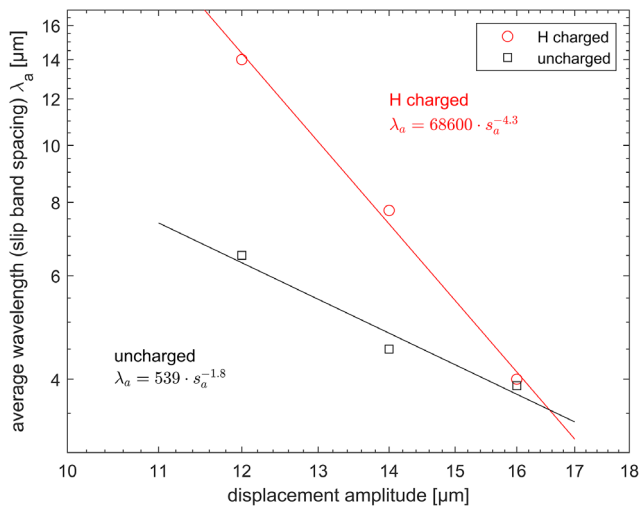


Figure 6. Evolution of slip band spacing, the distance between intrusions and extrusions, represented by the average wavelength λ_a of extracted profiles from AFM data for a given displacement amplitude and corresponding fits.

As shown in **Figure 6**, the evolution of the slip band spacing, represented by λ_a , with the applied displacement amplitude s_a follows a power law

Table 2. Parameters of power law fit of slip band spacing, represented by λ_a , and applied displacement amplitude s_a .

Fit parameters	Uncharged	H charged
n	1.791	4.341
λ_a	6.86×10^5	539

$$\lambda_a = k_\lambda \cdot s_a^{-n} \quad (1)$$

The parameters of the power-law fit are given in **Table 2**. The difference in the slip band spacing decreased with increasing displacement amplitude, starting from below 50% to almost 0 at the last evaluable displacement amplitude.

4.2. Slip Irreversibility

While in f.c.c. materials, slip lines and bands appear more prominent in the presence of hydrogen,^[43] this is not the case for b.c.c. low-carbon steels. Mine et al. observed that the slip band height throughout fatigue at one load level up to 40 000 load cycles in the presence of hydrogen is only 54% compared to the uncharged reference case.^[35] A similar behavior can be confirmed in this study. As shown in **Figure 4**, across all displacement amplitudes,

the slip line height in the H charged case is lower than in the reference specimen, where the value of 54% measured by Mine et al. can be confirmed within the large scattering of measurements. Mine et al. attributed this to a reduced slip irreversibility in the presence of hydrogen without further experimental evidence. Hydrogen reduces kink formation energy^[7] and increases kink motion energy by a solute drag effect,^[44] whereby the latter dominates at high hydrogen concentrations. Since we electrochemically charge to high hydrogen concentrations over several days, it can be assumed that we have very high hydrogen concentrations locally at the surface. As already mentioned in the introduction section, hydrogen changes the structure of the dislocation core and reduces the slip anisotropy of the b.c.c. screw dislocations.^[19] Therefore, dislocation motion becomes more flexible also with respect to cross-slip. It can thus be assumed that those processes that lead to the formation of the dislocation cell structure are strongly influenced by the mobility of the dislocations even out of their slip plane. If dislocation slip is more flexible, orientation gradients could annihilate more easily. The slip reversibility could increase, then. This was shown in Figure 5. The cell walls are obviously less prominent in the STEM image in the presence of hydrogen. The histograms of the misorientations show, as do the KAM maps, that orientation gradients are less prominent in the H-charged specimens for all given displacement amplitudes.

5. Conclusion

The effect of hydrogen on cyclic plasticity, on the evolution of slip bands, and their spacing were investigated for high-purity ferritic iron. This investigation focused on orientation gradient formation during fatigue. It can be concluded that: 1) The spacing of slip bands is increased by the presence of hydrogen, whereas their height is decreased significantly. The first is attributed to slip localization and hence to the HELP mechanism; 2) For large displacement amplitudes, the slip band spacing coincides for both cases, the H charged and the uncharged case, while the slip band height remains different; and 3) The dislocation cell structure differs from f.c.c. materials. The dislocation cells are less pronounced in the presence of hydrogen. In combination with the less prominent intrusions and extrusions, this is ascribed to less slip anisotropy. Experimental evidence is given for hydrogen to reduce the slip irreversibility.

However, Seeger and Wasserbaech^[45] had argued that interstitials, like hydrogen, could shift the transition temperature at which {110} slip in b.c.c. materials changes to {112}-slip from low to a higher temperature. This could also be the underlying mechanism for the modification in the dislocation cell structure, but requires further detailed investigation, e.g., by TEM tomography, in future work.

Acknowledgements

The authors kindly acknowledge the assistance of Christoph Pauly and Joerg Schmauch from Saarland University during lift out of the lamellas and the transmission kikuchi diffraction.

Open Access funding enabled and organized by Projekt DEAL.

Conflict of Interest

The authors declare no conflict of interest.

Data Availability Statement

The data that support the findings of this study are available from the corresponding author upon reasonable request.

Keywords

α -iron, hydrogen, in situ fatigue, persistent slip band, slip reversibility

Received: December 30, 2022

Revised: March 1, 2023

Published online: March 22, 2023

- [1] X. Li, X. Ma, J. Zhang, E. Akiyama, Y. Wang, X. Song, *Acta Metal. Sin.* **2020**, *33*, 759.
- [2] P. Gruenewald, N. Hautz, C. Motz, *Int. J. Hydrogen Energy* **2022**, *47*, 15922.
- [3] A. P. A. Subramanyam, A. A. Guzmán, S. Vincent, A. Hartmaier, R. Janisch, *Metals* **2019**, *9*, 291.
- [4] A. A. Guzmán, J. Jeon, A. Hartmaier, R. Janisch, *Materials* **2020**, *13*, 5785.
- [5] W. H. Johnson, *Proc. R. Soc. London* **1875**, *23*, 168.
- [6] T. Tabata, H. K. Birnbaum, *Proceedings of Yamada Conference IX* (Eds: H. Suzuki, K. Sumino, S. Takeuchi, T. Ninomiya), University of Tokyo Press **1985**, p. 219.
- [7] H. Matsui, H. Kimura, S. Moriya, *Mater. Sci. Eng.* **1979**, *40*, 207.
- [8] H. K. Birnbaum, P. Sofronis, *Mater. Sci. Eng. A* **1994**, *176*, 191.
- [9] A. S. Ebner, E. Plesiutchnig, H. Clemens, R. Pippan, V. Maier-Kiener, *Int. J. Hydrogen Energy* **2021**, *46*, 38132.
- [10] D. Delafosse, J.-P. Chateau, A. Chambreuil, T. Magnin, *Mater. Sci. Eng. A* **1997**, *234*, 889.
- [11] Y. Jagodzinski, H. Hänninen, O. Tarasenko, S. Smuk, *Scr. Mater.* **2000**, *43*, 245.
- [12] P. J. Ferreira, I. M. Robertson, H. K. Birnbaum, *Acta Mater.* **1998**, *46*, 1749.
- [13] P. J. Ferreira, I. M. Robertson, H. K. Birnbaum, *Acta Mater.* **1999**, *47*, 2991.
- [14] P. J. Ferreira, I. M. Robertson, H. K. Birnbaum, *Mater. Sci. Forum* **1996**, *207–209*, 93.
- [15] Y. You, Q. Teng, Z. Zhang, Q. Zhong, *Mater. Sci. Eng. A* **2016**, *655*, 277.
- [16] G. Lu, Q. Zhang, N. Kioussis, E. Kaxiras, *Phys. Rev. Lett.* **2001**, *87*, 095501.
- [17] I. M. Robertson, *Eng. Fract. Mech.* **1999**, *64*, 649.
- [18] S. Taketomi, R. Matsumoto, N. Miyazaki, *J. Mater. Sci.* **2008**, *43*, 1166.
- [19] S. Wang, N. Hashimoto, S. Ohnuki, *Sci. Rep.* **2013**, *3*, <https://doi.org/10.1038/srep02760>.
- [20] M. L. Martin, M. Dadfarnia, A. Nagao, S. Wang, P. Sofronis, *Acta Mater.* **2019**, *165*, 734.
- [21] C. Buque, *Int. J. Fatigue* **2001**, *23*, 459.
- [22] U. Essmann, U. Gösele, H. Mughrabi, *Philos. Mag. A* **1981**, *44*, 405.
- [23] M. Marx, W. Schaef, M. T. Welsch, *Int. J. Fatigue* **2012**, *41*, 57.
- [24] F. Schäfer, E. P. W. Lang, M. Bick, A. F. Knorr, M. Marx, C. Motz, *Proc. Struct. Integrity* **2017**, *5*, 547.
- [25] J. Man, K. Obrtlík, J. Polak, *Philos. Mag.* **2009**, *89*, 1295.
- [26] H. Mughrabi, *Metall. Mater. Trans. B* **2009**, *40*, 431.

- [27] M. Petre nec, J. Polák, K. Obrtík, J. Man, *Acta Mater.* **2006**, *54*, 3429.
- [28] B. Šesták, V. Novák, S. Libovický, *Philos. Mag. A* **1988**, *57*, 353.
- [29] H. J. Roven, E. Nes, *Acta Metall. Mater.* **1991**, *39*, 1719.
- [30] H. Mughrabi, K. Herz, X. Stark, *Int. J. Fracture* **1981**, *17*, 193.
- [31] K. Pohl, P. Mayr, E. Macherauch, *Scr. Metall.* **1980**, *14*, 1167.
- [32] C. Sommer, H. Mughrabi, D. Lochner, *Acta Mater.* **1998**, *46*, 1527.
- [33] D. V. Wilson, J. K. Tromans, *Acta Metall.* **1970**, *18*, 1197.
- [34] S. Wang, A. Nagao, P. Sofronis, I. M. Robertson, *Acta Mater.* **2019**, *174*, 181.
- [35] Y. Mine, J.-M. Olive, K. Nagata, T. Mitsutani, *Mater. Sci. Eng. A* **2011**, *528*, 8090.
- [36] Z. Ma, X. Xiong, L. Chen, Y. Su, *Electrochim. Acta* **2021**, *366*, 137422.
- [37] C. Müller, M. Zamanzade, C. Motz, *Micromachines* **2019**, *10*, 114.
- [38] A. S. Ebner, S. Brinckmann, E. Plesiutchnig, H. Clemens, R. Pippan, V. Maier-Kiener, *JOM* **2020**, *72*, 2020.
- [39] M. Asadipoor, A. P. Anaraki, J. Kadkhodapour, S. M. H. Sharifi, A. Barnoush, *Mater. Sci. Eng. A* **2020**, *772*, 138762.
- [40] M. Asadipoor, A. Barnoush, *Int. J. Hydrogen Energy* **2022**, *47*, 10112.
- [41] D. Cereceda, M. Diehl, F. Roters, D. Raabe, J. M. Perlado, J. Marian, *Int. J. Plast.* **2016**, *78*, 242.
- [42] W. Pantleon, N. Hansen, *Acta Mater.* **2001**, *49*, 1479.
- [43] D. P. Abraham, C. J. Altstetter, *Metall. Mater. Trans. A* **1995**, *26*, 2859.
- [44] R. Kirchheim, *Scr. Mater.* **2012**, *67*, 767.
- [45] A. Seeger, W. Wasserbäch, *Matér. Tech.* **2003**, *91*, 51.